Test report on the

SITe ST-002 camera
for HFOSC

Anton Norup Sørensen
IJAF, Copenhagen University Observatory

January 2001

Contents

1 Introduction

This report presents the results from characterization of the CCD camera built by Copenhagen University Observatory, to be used with the "HFOSC". The detector is a SITe ST-002 CCD. Some data on the engineering grade array are also included in this report, where these are compared to the science grade array.

The CCD has an imaging area of 2048 by 4096 pixels, each 15μm side length, and is thinned and backside illuminated. The array is significantly larger than the entrance window of the camera, which means than only the central area can be characterized.

The detector has two output amplifiers. A single amplifier can be used, or the two can be used simultaneously.

2 Cosmetics

Flat fields for wavelengths of 1060nm, 550nm and 334nm are shown in figures 1, 2 and 3, respectively. Only the central 2048 by 2048 pixels are shown, as vignetting from the window occurs just outside this region.

At visible wavelengths, exemplified by 550nm, uniformity of the flat field is relatively good. Over most of the area, large scale variations are within $\pm 2\%$. Near the right edge, sensitivity rises by 10% above average. Close to the center of the field, there is a spot about 20 pixels in diameter where the QE drops to about 60% of average in the center. Hundreds of circular spots with a diameter of 8 pixels are present all over the area. The sensitivity drop in the spots varies, but is rarely more than 5%.

Going to 334nm, many artifacts faintly visible at 550nm, now stand out clear. A cross in the middle, and zig-zag patterns at both sides stand out by about 2%. Overall sensitivity variations are about $\pm 4\%$, increasing to 10% at the sides. The dark and bright spots already seen at 550nm now are stronger, several deviating more than 10%.

At 1060nm, the extreme long wavelength end of the sensitivity range, QE uniformity is degrading. In the central region, variations are about $\pm 4\%$, and the sensitivity drops by about 10% at both sides. The bright spot in the center of the field is due to scattered light in the characterization setup.

Charge traps and bad columns can be found by comparing a flat field exposure at very low illumination level to a well exposed one, as illustrated in figure 4. Several exposures at 70e- and 59Ke- were combined to produce two high S/N flat field maps for the comparison.

Strictly speaking, the CCD has no bad columns, but is has charge traps so deep that they have about the same effect as a bad column. A list of the found traps is shown below. The depth of each trap is estimated from the number of pixels affected in the low level flat field. Data in the columns coinciding with traps marked as deep may be necessary to discard.

Trap location	**Approx. depth**
$[54, *]$	Low level, deep trap
$[134, *]$	Low level, deep trap
$[1760, 2224]$	$100e^-$
$[1813 : 1814, *]$	All levels, very deep trap
$[1960, 2077]$	$300e^-$
$[1994, 2115]$	$100e^-$
$[2055, 1610]$	$150e^-$

3 Read-out noise

The following table shows the read-out noise (RON) found in different amplifier configurations.

	Amplifier A	Amplifier B
High gain:	4.8 e^-	5.1 e^-
Low gain:	8 e^-	8 e^-

A slight pattern from electronic pick-up noise was visible in all conditions, but when the camera was properly de-coupled from external noise sources, this was with an amplitude far less than the white noise of the read-out amplifier.

The reason for the higher noise in low gain mode is undersampling of the noise caused by the conversion factor of 5.6 e^-/ADU.

As reading out through a single amplifier is usually preferred for simplicity of reductions, amplifier A is recommended due to the slightly lower RON.

4 Gain, linearity and full-well

Gain, the conversion factor between Analog to digital units (ADU) and electrons was determined in two ways: By analysis of photon noise statistics, and by illumination with Fe-55 X-rays of known energy. The following conversion factors were found:

Gain	Method	Amplifier A	Amplifier B
High gain	Fe55	1.22e^-/ADU	1.21e^-/ADU
High gain	Poisson	1.24e^-/ADU	1.22e^-/ADU
Low gain	Poisson	5.6 e^-/ADU	5.6 e^-/ADU

Fe-55 gain measurements were made at -100°C and -80°C, and gave identical values for gain at both temperatures. The Fe-55 method is far more precise than noise analysis, so the values from this method should be used for high gain.

An example of gain determination from Poisson noise is shown in the upper part of figure 5. Here the gain is determined from the approximately constant level measured over a wide illumination range.

Gain determination from noise analysis is rarely precise enough for linearity measurements. In stead, linearity deviations are examined by measuring the ADU level versus exposure time, using a stable light source. Measurements made in this way on amplifier A are plotted in the lower half of figure 5. By dividing the counts with the exposure time, corrected for shutter delay, a linear response should result in a constant level. Linearity was mapped from approximately $200e^-$ to $60Ke^-$, and shows a systematic $\pm 0.5\%$ deviation. For high precision photometry, this should be compensated for during reductions. The behavior of amplifier B was found to be the same as A.

The onset of full well is also visible in figure 5, as a sudden increase in gain and a drop in counts per second. As the gain deviation is the most sensitive indicator, this was used to determine full well.

With default voltages, the full well was found to be quite low, about $52Ke^-$, and very dependent on the location on the detector. The clocking speed and phase voltages was then tuned to maximize the full well. For both amplifiers, this resulted in a final full well of $51KADU \approx 62Ke^-$ in MPP mode, and a full well of $59KADU \approx 72Ke^-$ in non-MPP mode. The difference in full well of the two modes is shown in figure 6.

For an acceptable full well, quite slow clocking of the phases is required. This means that clearing the detector before an exposure takes 20 seconds, and read-out of a full frame takes 165 seconds.

The appearance of onset of saturation in the image changed during the optimization process, from smearing of the signal to individual columns deviating before others.

It is interesting to note that while the science grade CCD required considerable adjustment to reach a full well close to specifications, the engineering grade device had a full well of $70Ke^-$ with default setup.

Due to the low full well, the high gain mode is adequate to sample the full dynamic range, and the low gain mode does not have any practical use.

5 Charge Transfer Efficiency

The fraction of electrons that are successfully moved from one pixel to another during read-out is described by the charge transfer efficiency (CTE).

The CTE has been measured using a ^{55}Fe X-ray source, whose emissions generate a specific number of photo-electrons on the CCD for each detection. The read-out counts as a function of position on the CCD can then be converted to a CTE value. Measurements were made at detector temperatures of -80°C and -100°C and were found to be unchanged with temperature.

The values found for the two read-out directions are:

	Amplifier A	Amplifier B
Serial CTE:	0.999999	0.999999
Parallel CTE:	1.000000	0.999999

These values are, with an uncertainty of about $2 \cdot 10^{-6}$, indistinguishable from perfect CTE.

Note that CTE strictly speaking is a function of exposure level, so the value given here may not be applicable to all cases. Near zero level and full well, CTE may be poorer than the value given here.

6 Modulation Transfer Function

Data for measurement of the Modulation Transfer Function have been collected by measuring the contrast of fringes of different spatial wavelength projected onto the CCD. The results are shown in figure 7, along with MTF measurements on a Loral 2K3EB backside illuminated CCD and an EEV CCD 44-82. A curve for the pixel geometry MTF is also shown.

The SITe CCD has a very good MTF, although not as good as the EEV device, while the Loral detector performs far worse. The illumination wavelength was 670nm, at which the absorption depth is relatively small. A backside illuminated device with a significant internal field free region will suffer from charge diffusion, degrading the MTF. Apparently, the SITe and EEV device have a much smaller field free region than the Loral. All measurements are still far below the ideal pixel MTF response. A direct comparison to the theoretical value should be made with caution, as the measurements have not been corrected for the slit width of the projector and other error sources. In general, the actual MTF can be expected to be slightly higher than the displayed measurement results.

7 Quantum-efficiency

Quantum efficiency vs. wavelength and temperature:

The sensitivity has been measured through 11 narrow-band filters from 334nm to 1060nm and is plotted in figure 8. The data were extracted from an area of 400 by 400 pixels near the center of the detector.

As already found for other SITe CCDs, type ST-005A, this detector of type ST-002 has a distinct temperature dependency of the quantum efficiency (QE). The effect was very pronounced for the engineering grade array, which was tested at temperatures between -120°C and -80°C. Surprisingly, the engineering grade array was found to have higher QE than the science grade array.

The science grade CCD had QE measured at -100°C and -80°C. Especially at short wavelengths, there is an advantage from increasing the operating temperature. Operating at -80°C will usually require MPP mode to suppress dark current. The increase in dark current or the loss in full well from MPP mode will usually be an acceptable price for the increased QE.

As the CCD becomes partially transparent at near-infrared wavelengths, interference from internal reflections may cause rapid variations in QE with position and wavelength. A flat-field was obtained with 830nm monochromatic illumination, and no fringes were seen. This indicates that the detector is very well suited for NIR imaging and spectroscopy.

Stability of the sensitivity:

QE was measured twice at each temperature, about 6 days apart, where the detector has been heated to room temperature and the cryostat has been opened twice in between. As shown in figure 8, there is a slight, but significant change. This is examined more closely below.

A degrading QE is unlikely to appear at a uniform rate over the detector. The most efficient method for checking QE stability is therefore to examine the differences in flat fields obtained some time apart. The change in local structure can be examined in figure 1 for 1060nm light, figure 2 for 550nm and figure 3 for 334nm. These flat fields were made simultaneously with the QE measurements, i.e. 6 days apart.

Especially visible in the 1060nm ratio image, it is clear that the illumination geometry has changed somewhat, creating a dumbbell like structure. Ignoring that, the 1060nm QE appears to be completely unchanged, while there are increasingly strong changes at shorter wavelengths. At 334 nm, spots with high and low sensitivity have changed QE by about 2%, and the cross-shaped structure has changed by 1

Changes in QE structure due to temperature changes were also examined. In exposures made at detector temperatures of -100°C and -80°C about two hours apart, the QE had changed by about 1% in the irregular dark diagonal pattern that can be seen in the 334nm flat.

8 Bias and overscan

The overall bias structure is flat and featureless. No local defects, like hot columns, are present.

The serial register is extended by 25 pixels in both directions, providing exposures with pre- and postscan regions. In addition, artificial overscan regions can be created by clocking beyond the physical pixels.

The overscan regions have proved quite reliable, making accurate bias subtraction possible. There still seems to be a slight influence on the bias level from the exposure level, but it only shifts one ADU per 40 KADU of exposure.

9 Dark current

In order to minimize dark current, the detector can be operated at a temperature of -100°C. In addition, the detector design allows for Multi-Pinned-Phase operation, which further reduces the dark current. By default, the voltages are set for MPP mode.

As demonstrated, higher operating temperature can improve quantum efficiency, but at a cost of increased dark current. To make the observer able to choose the optimal temperature, dark current has been examined at -100°C and -80°C. While MPP mode reduces dark current, non-MPP operation provides a higher full well. In all, the optimal combination of temperature and MPP selection depends on the application.

Given below is the dark current found in MPP and non-MPP mode, found from examining the level in several half-hour dark exposures.

Mode	**-100°C Dark current**	**-80°C Dark current**
MPP	0.3 $e^-/h \pm 0.5e^-/h$	2.0 $e^-/h \pm 0.5e^-/h$
Non-MPP	2.0 $e^-/h \pm 0.5e^-/h$	11 $e^-/h \pm 2e^-/h$

The dark current is not significantly detected in the MPP exposures at -100 °C, but becomes clear at higher temperature and / or non-MPP mode. Even in a non-MPP exposure of one hour at -80 °C, the shot noise from the dark current is lower than the read-out noise.

With MPP active, no features are visible in dark exposures. At -80°C, non-MPP mode, a few artifacts appears, as shown in figure 9. Relatively few warm pixels appears. Also, there is a vertical variation in the dark current level. This is most likely due to small scale bias level variations, and may be possible to correct by tracking the overscan level.

10 Cryostat

The detector cooling is provided by a thin braid connecting the CCD and a liquid Nitrogen (LN2) tank. Both are kept in an evacuated container. The pressure in the cryostat should be 10^{-5}mBar or lower when LN2 is present in the tank. Otherwise, the camera should be heated to room temperature and pumped. The LN2 holding time depends on the selected detector temperature, cryostat orientation and ambient temperature. With an ambient temperature of 22°C, the LN2 filling hole pointing upwards, and a detector temperature of -100°C, the holding time is 29 hours. With a CCD temperature of -80°C, the holding time decreases to 26 hours.

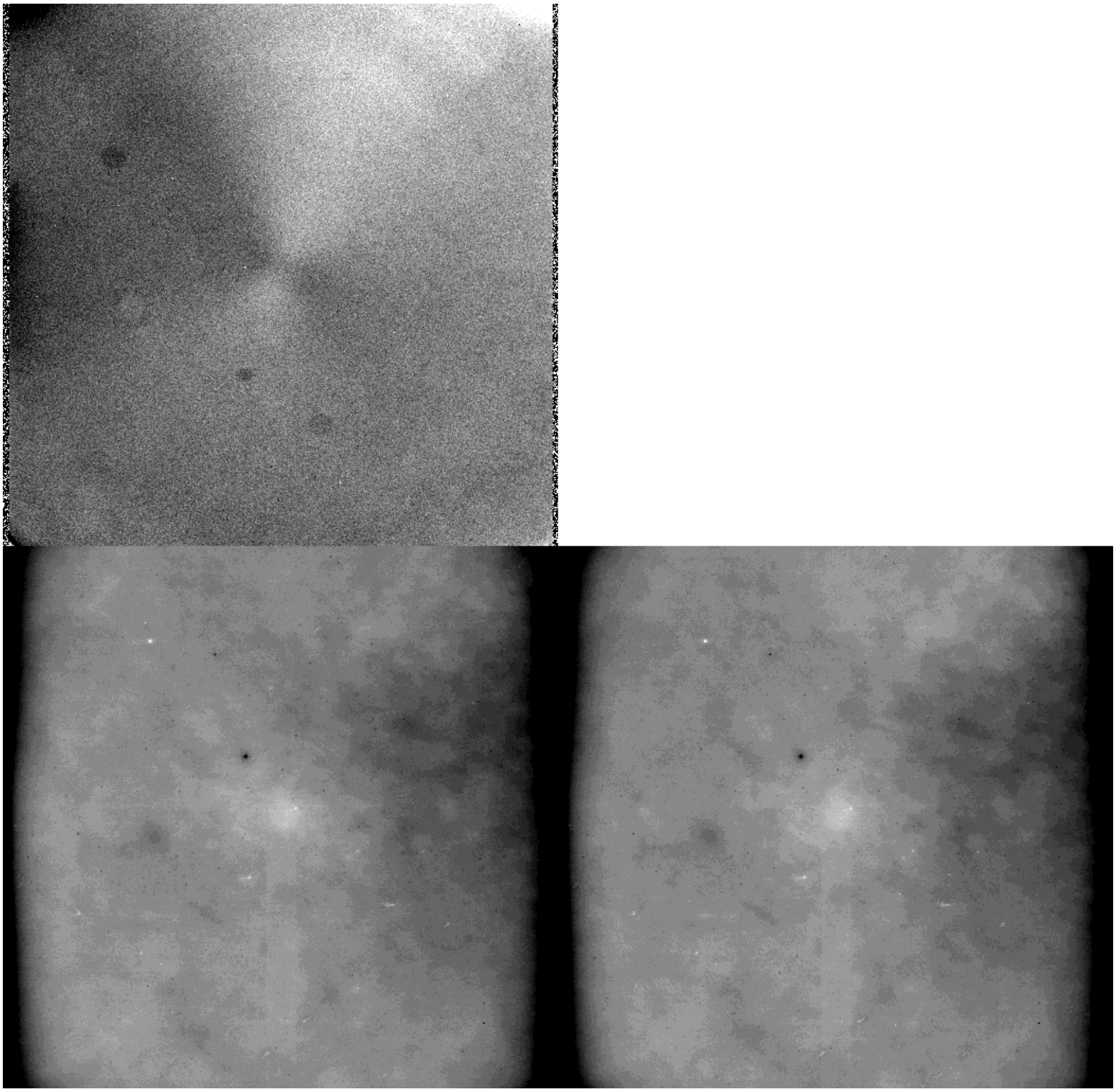

Figure 1: Flat field properties at 1060nm. *Lower left:* The greyscale cuts are set to ±10% of the median level. The large scale structure varies with a peak to peak amplitude of about 10%. This relates to the thickness of the CCD, almost completely transparent at this wavelength. *Lower right:* 6 days later, the structure is unchanged, although the cryostat has been opened twice in between. *Top:* Ratio between the two flat fields, displayed with cuts of ±2%. The illumination geometry can be seen to have changed, and a few specks of dust have moved. Otherwise, no changes can be detected.

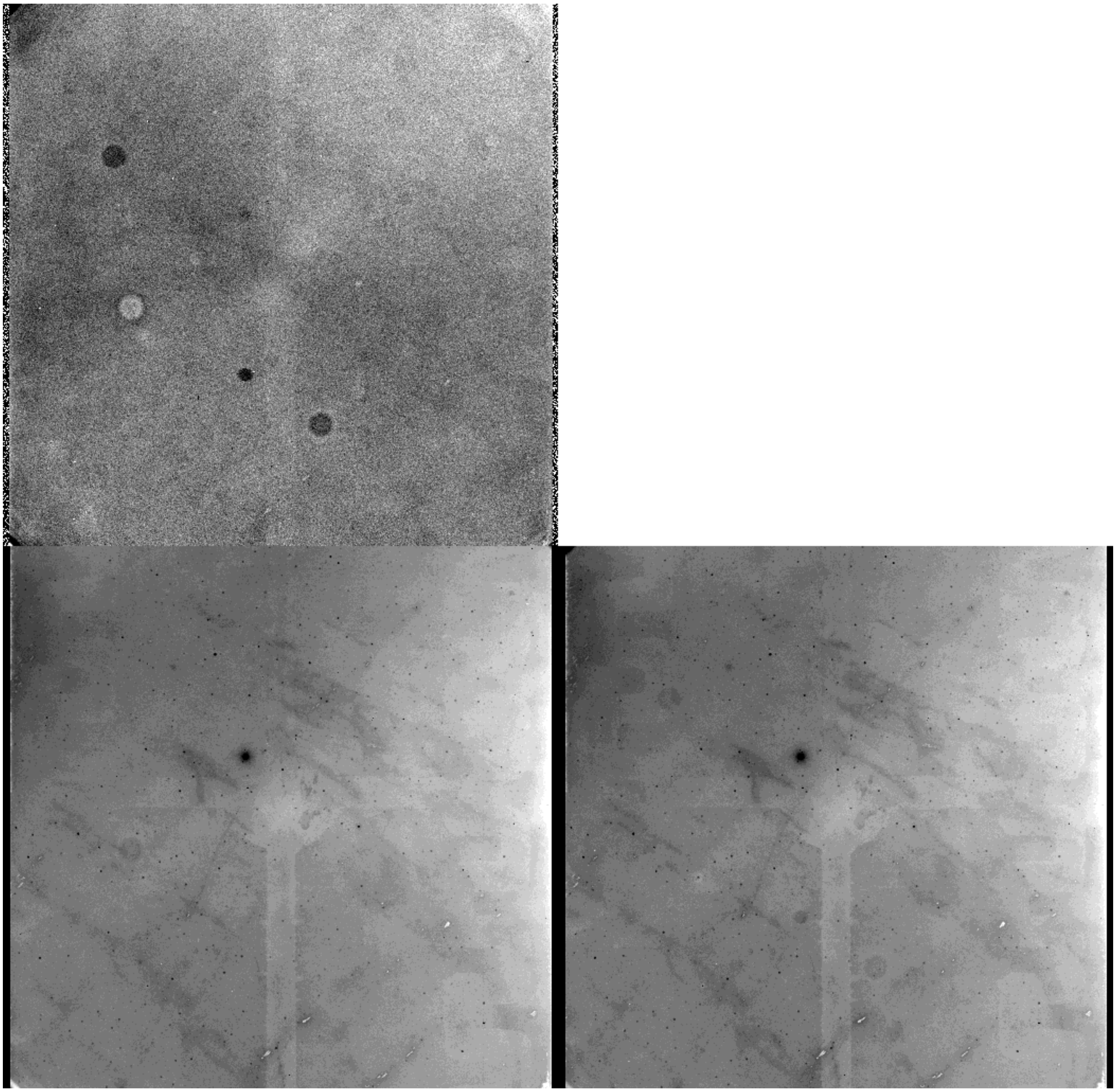

Figure 2: Flat field properties at 550nm. *Lower left:* The greyscale cuts are set to ±10% of the median level. Uniformity is relatively good at this wavelength. Peak to peak large scale structure is generally about 4%, increasing to 10 % at the right edge. *Lower right:* 6 days later, the structure is unchanged. *Top:* Ratio between the two flat fields, displayed with cuts of ±2%. Apart from tiny clusters of pixels in regions with abnormal sensitivity, stability of the flat field is good.

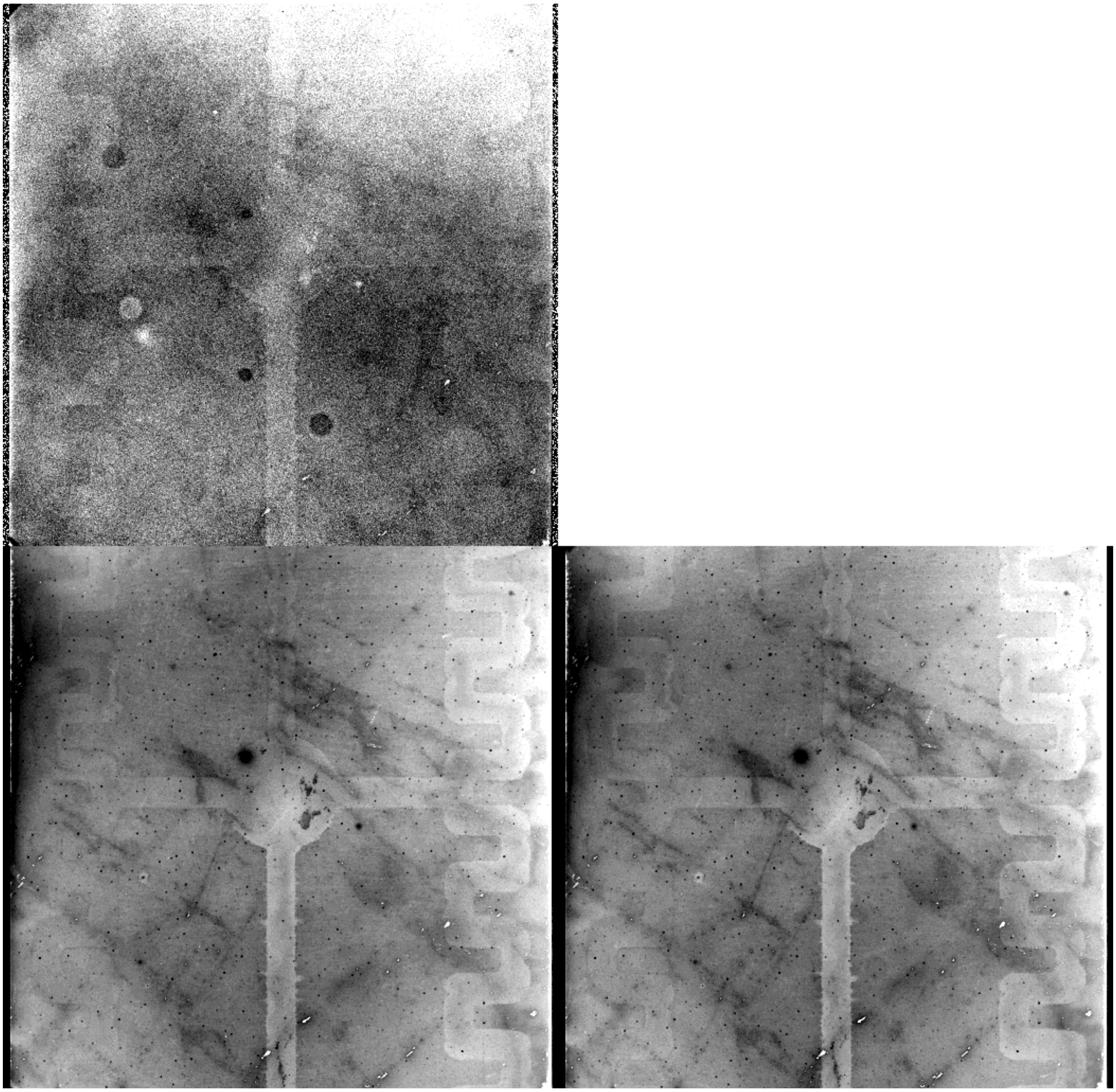

Figure 3: Flat field properties at 334nm. *Lower left:* The greyscale cuts are set to $\pm 10\%$ of the median level. Irregularities are quite strong, originating form surface defects and the manufacturing process. *Lower right:* 6 days later, the structure is generally similar. *Upper left:* Ratio between the two flat fields, displayed with cuts of $\pm 2\%$. The apparent large scale variations are due to changes in illumination. Real changes are seen in small spots with unusual low or high sensitivity in the flat field. Also, the sensitivity of the cross pattern has changed slightly.

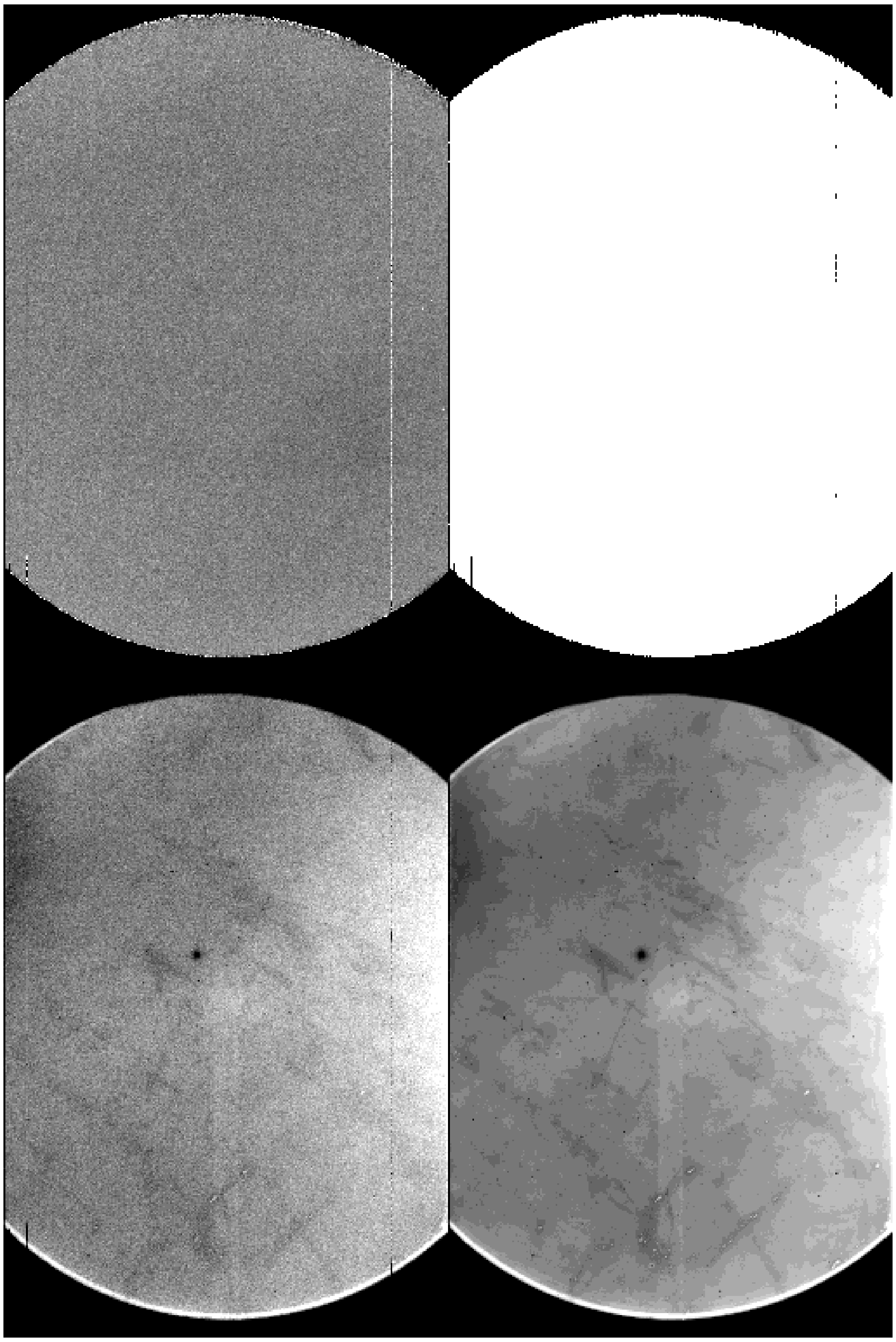

Figure 4: Comparison of a 550nm high and low illumination flat field, in order to identify charge traps. These exposures include a larger fraction than previous images of the detector in the vertical direction, and thereby show the vignetting of the window. *Lower left:* Flat field at an illumination level of $70e^{-}$/pixel. Grey scale cuts are $\pm$ 10% of median level. A few columns with bad charge transfer can be seen. *Lower right:* Flat field at an illumination level of $39.000e^{-}$/pixel. Grey scale cuts are $\pm$ 10% of median level. *Upper left:* Ratio of the two flat fields. Grey scale cuts are $\pm$ 10% of median level.
A bad column stands out, along with partly bad columns in the lower left part. Small traps are visible as white dots near the right border.

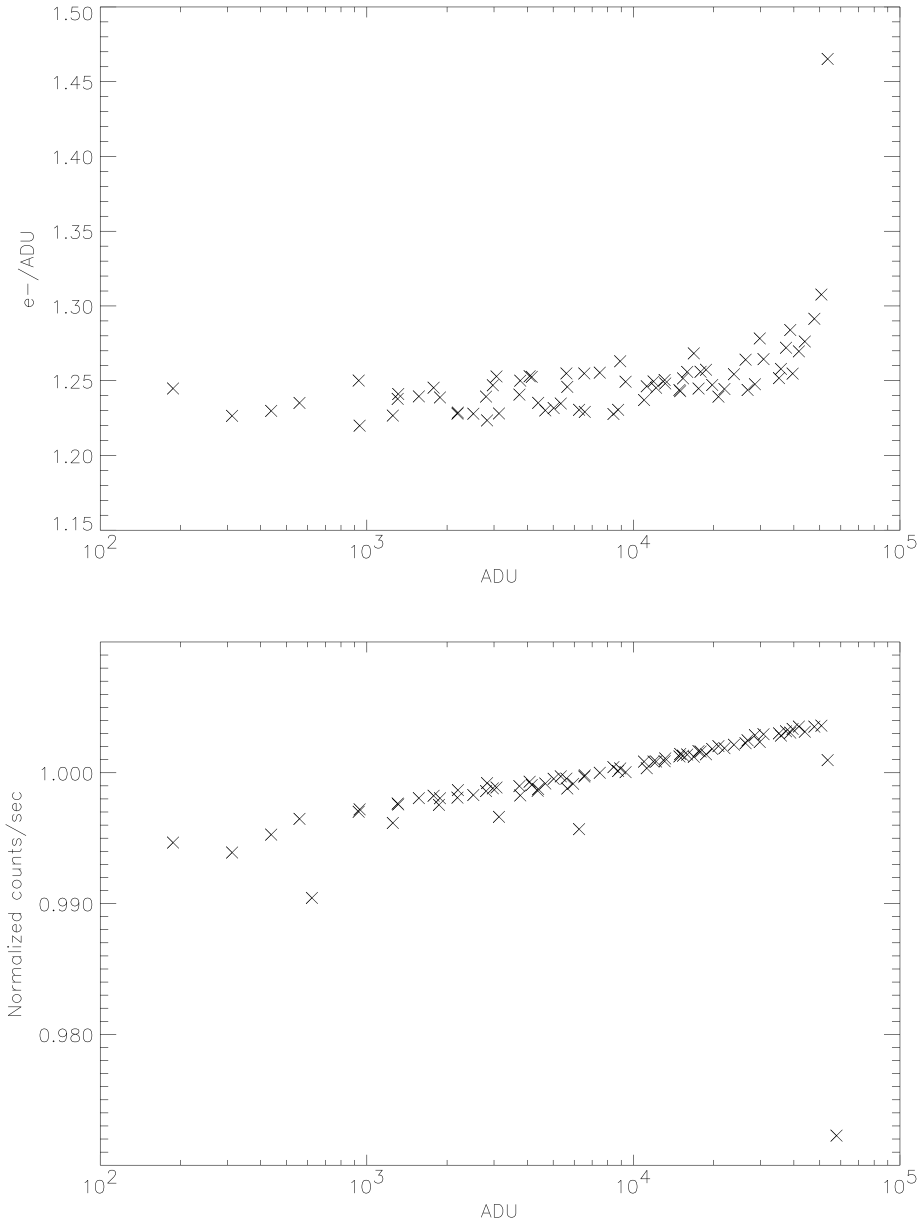

Figure 5: *Top:* Gain versus exposure level measured from noise statistics for amplifier A in high-gain, mpp mode. *Bottom:* A plot of ADU per second versus total exposure time, corrected for shutter delay. Amplifier A in high-gain, mpp mode was used.

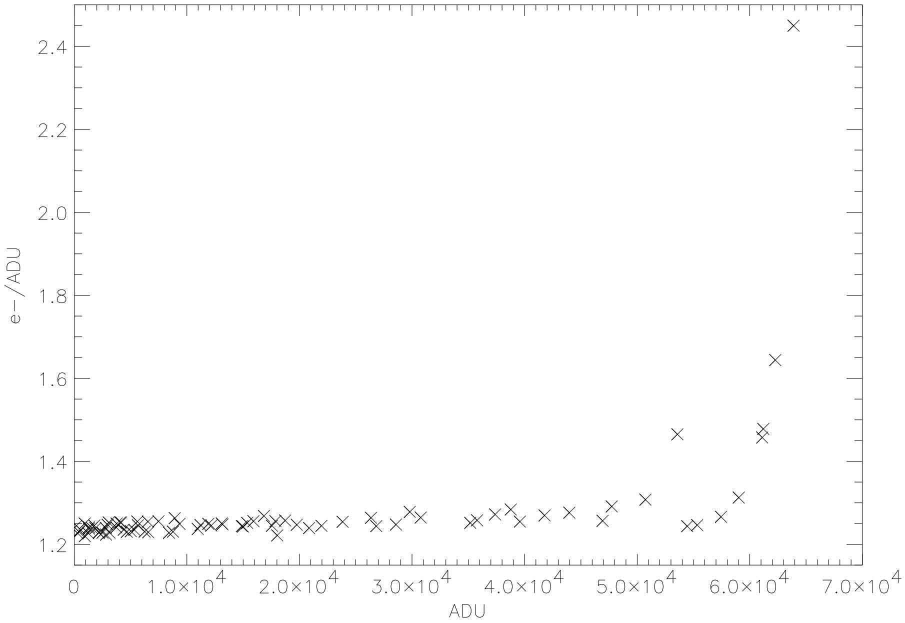

Figure 6: Gain versus exposure level measured from noise statistics for amplifier A in high-gain mode. Data from mpp and non-mpp mode are merged. The mpp points are deviating from linearity slightly above 50KADU, and the non-mpp data are deviating at a higher level, about 60KADU.

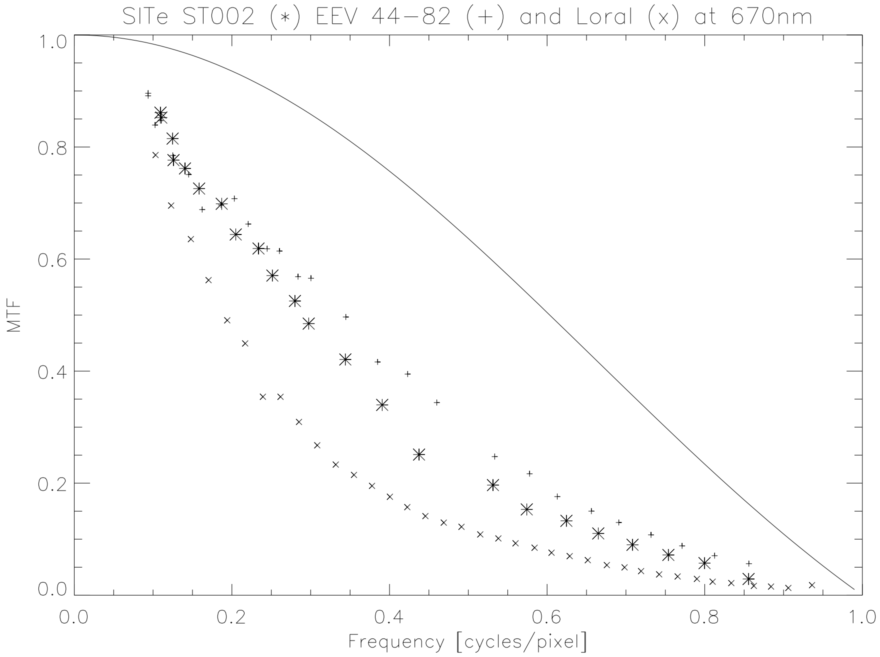

Figure 7: Modulation Transfer Function measurement of the SITe ST-002, compared to measurements on EEV and Loral CCDs and the ideal pixel response.

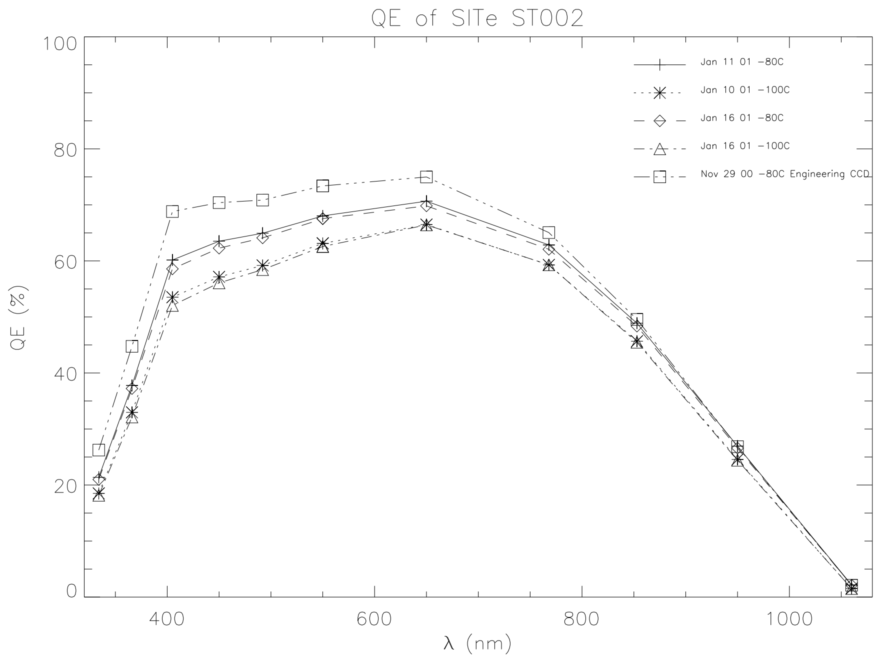

Figure 8: Global quantum efficiency versus wavelength for the SITe ST-002 CCD, measured from the sigma-clipped mean of the central area of a flat field exposure. Measurements at -100°C and -80°C are shown to illustrate temperature dependency of QE. For each temperature, measurements are made about 6 days apart, to show the stability of the sensitivity. For comparison, the QE of the engineering grade array is included.

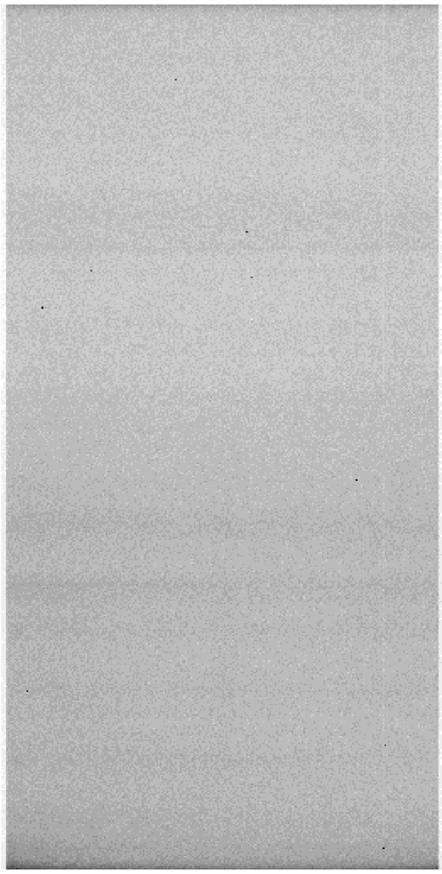

Figure 9: A median-combined image of six 30 minute dark exposures at a detector temperature of -80°C, non-MPP mode. Grey-scale cuts are -2 to +20 ADU relative to the bias level. The increased background stands out from the pre- and post-scan regions at both sides. A few hot pixels are visible, and a slight variation in the dark current level occurs in horizontal bands.